NeuroImage 270 (2023) 119943

Contents lists available at ScienceDirect

NeuroImage

journal homepage: www.elsevier.com/locate/neuroimage

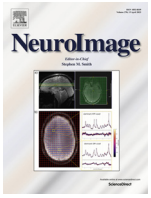

Hippocampus Modulates Vocalizations Responses at Early Auditory Centers

Alex T.L. Leong[a,b,*], Eddie C. Wong[a,b], Xunda Wang[a,b], Ed X. Wu[a,b,c,*]

[a] Laboratory of Biomedical Imaging and Signal Processing, The University of Hong Kong, Pokfulam, Hong Kong SAR, China
[b] Department of Electrical and Electronic Engineering, The University of Hong Kong, Pokfulam, Hong Kong SAR, China
[c] School of Biomedical Sciences, LKS Faculty of Medicine, The University of Hong Kong, Pokfulam, Hong Kong SAR, China

ARTICLE INFO

Keywords:
fMRI
Auditory system
Hippocampus
Inferior colliculus
Medial geniculate body
Auditory cortex
Optogenetics
Vocalizations

ABSTRACT

Despite its prominence in learning and memory, hippocampal influence in early auditory processing centers remains unknown. Here, we examined how hippocampal activity modulates sound-evoked responses in the auditory midbrain and thalamus using optogenetics and functional MRI (fMRI) in rodents. Ventral hippocampus (vHP) excitatory neuron stimulation at 5 Hz evoked robust hippocampal activity that propagates to the primary auditory cortex. We then tested 5 Hz vHP stimulation paired with either natural vocalizations or artificial/noise acoustic stimuli. vHP stimulation enhanced auditory responses to vocalizations (with a negative or positive valence) in the inferior colliculus, medial geniculate body, and auditory cortex, but not to their temporally reversed counterparts (artificial sounds) or broadband noise. Meanwhile, pharmacological vHP inactivation diminished response selectivity to vocalizations. These results directly reveal the large-scale hippocampal participation in natural sound processing at early centers of the ascending auditory pathway. They expand our present understanding of hippocampus in global auditory networks.

1. Introduction

In the central auditory system, auditory input from the ear transmits to the cochlear nucleus, superior olivary complex, inferior colliculus (IC), medial geniculate body (MGB) in thalamus, and auditory cortex (AC) along the ascending auditory pathway (Sitko and Goodrich, 2021, Schreiner and Winer, 2005, Malmierca, 2015). Information is hierarchically relayed along this ascending pathway, as distinct auditory features like amplitude and frequency are gradually extracted and processed throughout each auditory center (Malmierca, 2015, Chechik et al., 2006, Leaver and Rauschecker, 2010, Eggermont, 2001, Suga and Ma, 2003). Existing functional frameworks describing auditory processing in the ascending auditory pathway are often examined using basic stimuli such as pure tones and broadband noise (Kim and Doupe, 2011, Ono et al., 2017, Sturm et al., 2014). However, neural representation of simplified acoustic stimuli may not reliably predict responses to natural sounds (Kim and Doupe, 2011, Nagel and Doupe, 2008, Schneider and Woolley, 2011, Woolley et al., 2006), such as vocalizations, which are critical for facilitating communications and behavioral responses (Portfors, 2007, Woolley and Portfors, 2013, Simmons, 2003). Natural sound processing requires decoding complex spectrotemporal dynamic properties (Theunissen and Elie, 2014, Overath et al., 2015) and additional input from higher-order regions is needed to facilitate tacitly assumed auditory functions such as communication, learning, and memory processes (Zhang et al., 2018, Aronov et al., 2017, Guo et al., 2019, Xiao et al., 2018). Despite the current consensus on the pivotal roles played by AC corticofugal projections in natural sound processing (Suga and Ma, 2003, Winer, 2006, Xiong et al., 2015, Blackwell et al., 2020), emerging structural evidence has revealed that auditory midbrain and thalamus project to non-auditory regions such as superior colliculus (Lesicko et al., 2020) and striatum (Chen et al., 2019), respectively, and receive afferents from sensory, prefrontal, and limbic regions (Olthof et al., 2019, Marsh et al., 2002). These findings suggest that information can transmit in and out of early auditory centers in the ascending pathway to cortex and beyond, parallel with those at the AC level in the processing hierarchy. We hypothesize that the auditory network for natural sound processing is more brain-wide than presently known.

Given its roles in memory, emotion, and learning functions (Bird and Burgess, 2008, Buzsaki and Moser, 2013, Lisman et al., 2017), we contend that the hippocampus is a strong candidate to participate in brain-wide auditory processing of natural sounds. Notably, the hippocampus has been indirectly linked with auditory processing, whereby functional studies indicate interactions between the hippocampus and auditory cortex during learning and memory processes (Aronov et al., 2017, Terada et al., 2017). Electrophysiology studies demonstrate that the hip-

* Correspondence should be addressed to E.X. Wu or A.T.L. Leong, Laboratory of Biomedical Imaging and Signal Processing, Department of Electrical and Electronic Engineering, The University of Hong Kong, Pokfulam, Hong Kong, Hong Kong SAR, China. Fax: +852-2859-8738. Tel: +852-3917-7096.
E-mail addresses: tlleong@eee.hku.hk (A.T.L. Leong), ewu@eee.hku.hk (E.X. Wu).

https://doi.org/10.1016/j.neuroimage.2023.119943.
Received 26 January 2023; Accepted 13 February 2023
Available online 23 February 2023.

pocampus actively engages the auditory cortex to transform auditory inputs into long-term memories that are subsequently consolidated in cortical networks (Bendor and Wilson, 2012, Rothschild et al., 2017). Meanwhile, studies show that specific hippocampal neurons respond to sounds associated with a trained sound behavioral task (Xiao et al., 2018, Rothschild et al., 2017), implying that the hippocampus participates in the interpretation of complex auditory inputs. Anatomically, the hippocampus can receive and relay auditory signals via reciprocal projections directly with AC (Cenquizca and Swanson, 2007, Ohara et al., 2013) and indirectly through parahippocampal regions (van Strien et al., 2009, Oh et al., 2014) and forebrain pathways (Zhang et al., 2018, Munoz-Lopez et al., 2010), such as the entorhinal cortex, amygdala and medial septum complex. Tracing studies also indicated indirect projections, albeit scarcer, from the hippocampus to the IC and MGB via parahippocampal regions and amygdala (Olthof et al., 2019, Marsh et al., 2002, Cenquizca and Swanson, 2007). However, existing studies have not directly examined the role of the hippocampus in processing auditory inputs at these early auditory centers. Further, most studies so far focus on the cortex. They provide little to no evidence of the possible functional interactions between the hippocampus and auditory regions at the midbrain and thalamic levels. At present, whether and how the hippocampus functionally influences auditory responses, especially in the early ascending auditory centers, remains unknown.

Here, we posit that the hippocampus participates in natural sound processing at early sound processing centers within the ascending auditory pathway, especially the IC and MGB. The ventral hippocampus (vHP) plays a role in processing sensory inputs with an emotional context (Fanselow and Dong, 2010, Strange et al., 2014), thus it may influence natural sound processing throughout the ascending pathway. In this study, we examined whether optogenetically evoked vHP activity modulates sound processing in the auditory midbrain, thalamus and cortex. Using a combined optogenetic cell-specific stimulation of Ca^{2+}/calmodulin-dependent protein kinase IIα (CaMKIIα)-expressing vHP neurons in the dentate gyrus and whole-brain functional MRI (fMRI) visualization, we assessed blood-oxygenation-level dependent (BOLD) fMRI responses to two different categories of sound – natural sound (i.e., vocalizations) and artificial/basic acoustic stimuli. Here, two behaviorally relevant vocalizations (i.e., aversive and postejaculatory) representing opposite ends of the emotional valence (i.e., negative and positive), respectively, were chosen. We revealed that the vHP activity enhances auditory responses to both vocalizations, but not artificial stimuli or noise, in the IC, MGB and AC.

2. Methods

2.1. Subjects

Adult male Sprague-Dawley rats were used in all experiments. Animals were individually housed under a 12-h light/dark cycle with access to food and water ad libitum. All animal experiments were approved by the Committee on the Use of Live Animals in Teaching and Research of the University of Hong Kong. Group I (n = 10) underwent optogenetic fMRI experiments, group II (n = 11) underwent combined optogenetics and auditory fMRI experiments (n = 11, aversive vocalizations experiments; n = 10, postejaculatory vocalizations experiments; n = 8, broadband noise experiments), and group III (n = 7) underwent combined pharmacological and auditory fMRI experiments (only aversive vocalizations experiments). Two animals each from Group I and II, respectively, were selected at the end of the experiments for histological and immunohistochemistry brain slice preparation. Methodological details of histology and immunohistochemistry procedures can be found in our previous optogenetic fMRI studies (Leong et al., 2016, Chan et al., 2017, Leong et al., 2018, Wang et al., 2019, Leong et al., 2019, Leong et al., 2021).

2.2. Stereotactic Surgery for Viral Injection

Stereotactic surgery was performed when rats were 6 weeks old with bodyweight around 250 g (Leong et al., 2016, Chan et al., 2017, Leong et al., 2018, Wang et al., 2019, Leong et al., 2019, Leong et al., 2021). Injection was performed at two depths (-6.00 mm posterior to Bregma, +5.00 mm ML, -4.75 and -4.50 mm from brain surface) in the right/ipsilateral hemisphere in the dentate gyrus of vHP (Fig. 1A). 1.5 μL of viral constructs (i.e., AAV5-CaMKIIα-ChR2(H134R)-mCherry) were delivered through a 5 μL syringe and 33-gauge beveled needle injected at 150 nL/min at each depth. Following viral injection, the needle was held in the place for 10 minutes before slow retraction. Animals rested for six weeks before fMRI experiments were performed.

2.3. Optical Fiber Implantation and Animal Preparation for MRI Experiments

Stereotactic surgery was performed to implant custom made plastic optical fiber cannula (POF, core diameter 450 μm; Mitsubishi Super ESKA^{TM} CK-20) at the viral injection site 1 – 2 hours before fMRI experiments (Leong et al., 2016, Chan et al., 2017, Leong et al., 2018, Wang et al., 2019, Leong et al., 2019, Leong et al., 2021). Before implantation, the fiber tip was beveled to facilitate insertion and minimize injury to brain tissue. Then, it was inserted with the fiber tip at a depth of 4.7 mm. The optical fiber was fixed on the skull with UV glue and dental cement. The fiber outside the brain was made opaque using heat-shrinkable sleeves to avoid undesired visual stimulation (Leong et al., 2016, Chan et al., 2017, Leong et al., 2018, Wang et al., 2019, Leong et al., 2019, Leong et al., 2021). All MRI experiments were carried out on a 7T MRI scanner (PharmaScan 70/16, Bruker Biospin) using a transmit-only birdcage coil in combination with an actively decoupled receive-only surface coil. The animals were mechanically ventilated at a rate of 60 breaths per minute with 1% isoflurane in room-temperature air using a ventilator (TOPO, Kent Scientific) with continuous physiological monitoring. Vital signs were within normal physiological ranges (rectal temperature: 36.5 – 37.5°C, heart rate: 350 – 420 beat/min, respiration rate: 60 breath/min, oxygen saturation: > 95%) throughout the experiments.

2.4. MRI-Synchronized Optogenetic and Auditory Stimulation

An Arduino programming board synchronized the scanner trigger and the lasers for optogenetic and visual stimulation. Computers and light delivery systems were kept outside the magnet, and long optical patch cables (5–10 m) delivered light into the bore of the scanner. For optogenetic stimulation, blue light was delivered using a 473-nm DPSS laser. Light intensity was measured (PM100D, Thorlabs, USA) before each experiment as 8 mW at the fiber tip (450 μm, NA = 0.5), corresponding to a light intensity of 40 mW/mm^2. For auditory stimulation, acoustic stimuli were controlled by a computer and produced by a high frequency multi-field magnetic speaker (MF1, TDT) driven by an amplifier (SA1, TDT). Monaural stimulation was delivered through a custom-made 165 cm long rigid tube and a 6.5 cm soft tube into the animals' left/contralateral ear canal. The right/ipsilateral ear was occluded with cotton and Vaseline, to reduce the scanner noise reaching the ears. The sound pressure level (SPL) was measured by a recorder (FR2, Fostex, Japan) placed at ~ 2 mm from the tip of the soft tube. The variance of the light power was maintained less than 2.5 mW/mm^2 and the SPL less than 2 dB. This setup has been used in our previous studies (Leong et al., 2018, Leong et al., 2019, Gao et al., 2015).

To determine the frequency-dependent spatiotemporal characteristics of evoked vHP responses (optogenetic fMRI experiments), five frequencies were used (1 Hz, 5 Hz, 10 Hz, 20 Hz, and 40 Hz) with a light intensity of 40 mW/mm^2. 30 % duty cycle was used for all stimulation frequencies, except 1 Hz, which was at 10 % duty cycle. The duty cycle for 1 Hz optogenetic stimulation was reduced to avoid a very long

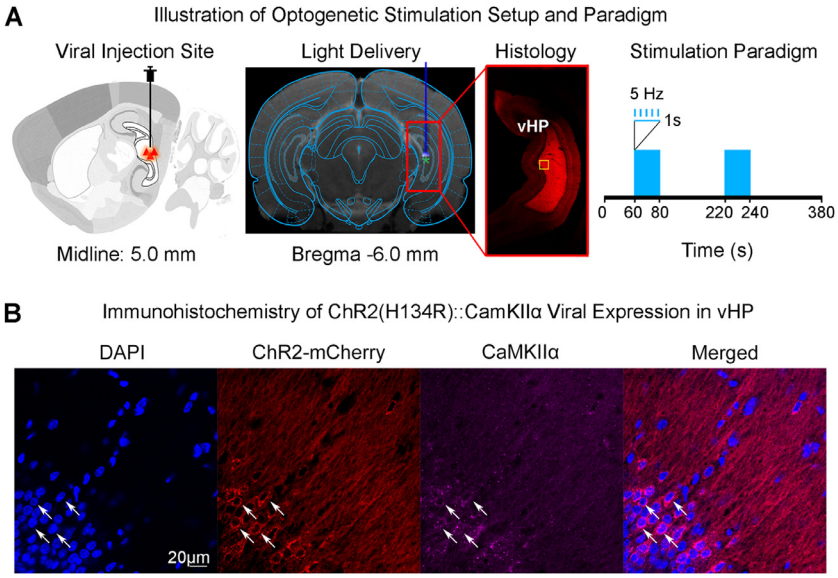

Fig. 1. Experimental setup for optogenetic stimulation and histological characterization of ChR2::CaMKII viral expression in ventral hippocampus (vHP) excitatory neurons. ***(A)*** Schematic *(Left)* and T2-weighted anatomical image *(Middle)* shows the viral injection and fiber implantation sites, respectively. Histology image shows viral expression in vHP (Red box). The yellow box indicates the location of magnified confocal images shown in *B*. Optogenetic fMRI stimulation paradigm *(Right)*. 5 Hz stimulation was presented at 30 % duty cycle in a block-design paradigm (20 seconds ON; 140 seconds OFF). ***(B)*** Merged representative confocal images co-stained for the nuclear marker DAPI, ChR2-mCherry, and excitatory marker CaMKIIα confirmed colocalization of ChR2-mCherry and CaMKIIα^+ neurons of vHP (white arrows).

stimulation pulse width which may not be physiological. vHP excitatory neurons were stimulated with a block design paradigm that consisted of 60 seconds light-off followed by 20 seconds light-on and 140 seconds light-off periods (**Supplementary Fig. 2A**). Three to four fMRI sessions were recorded for each frequency in an interleaved manner in each animal.

In combined optogenetic and auditory fMRI experiments, the effects of optogenetic stimulation in the vHP on brain baseline BOLD signals were first examined by presenting 5 Hz stimulation (60 seconds light-off followed by 20 seconds light-on and 140 seconds light-off periods), without presenting acoustic stimulation. This paradigm was repeated twice in each animal. Subsequently, the effects of optogenetic stimulation on auditory midbrain, thalamus, and cortex processing of sound stimulation were investigated. Here, the optogenetic stimulation (light wavelength: 473 nm, intensity: 40 mW/mm^2, pulse rate: 5 Hz, duty cycle: 30%) was continuously presented to the right vHP throughout the auditory fMRI sessions and alternated between sessions (**Supplementary Fig. 3A**). The choice of using a continuous optogenetic stimulation was made so that the modulatory effects upon vHP stimulation on BOLD fMRI responses to sound in the auditory centers can be characterized without mapping activations that directly resulted from optogenetic stimulation. This stimulation design choice was also made in our previous optogenetic fMRI study stimulating the hippocampus (Chan et al., 2017).

In the vocalization experiment, two types of vocalizations (I. 'Aversive' Vocalizations: bandwidth: 22-25 kHz, peak frequency: 22 kHz; sound pressure level (SPL): 83 dB, obtained online from http://www.avisoft.com/rats.htm (Gao et al., 2015); II. 'Postejaculatory' Vocalizations: bandwidth: 22 kHz, peak frequency: 22 kHz; SPL: 83 dB) from (Bialy et al., 2016) and their temporal reversions were presented. Aversive vocalizations are emitted by rats during distressing events (Gao et al., 2015) indicating negative emotional state, whereas postejaculatory vocalizations are emitted following copulation or in the presence of mating cues (Bialy et al., 2016) indicating positive emotional state. Standard block-design paradigm was used for the auditory stimulation (40 s sound-off followed by 4 blocks of 20 s sound-on and 40 s sound-off, fMRI no. of time points = 280) (**Supplementary Fig. 3A**). During every 20 s sound-on period, the aversive vocalization (length 1.2 s, plus silence 0.8 s afterward corresponding to 60 % duty cycle) (**Supplementary Fig. 3B**) was repeated ten times, whereas the postejaculatory vocalization (length 3.6 s, plus silence 0.4 s afterward corresponding to 90 % duty cycle) (**Supplementary Fig. 3B**) were repeated five times. For each animal, this paradigm was repeated six times for each type of vocalization sounds. For three of them, the forward vocalization was presented first; and for the other three, the reversed one was presented first (**Supplementary Fig. 3A**). Note that the forward and temporally reversed vocalizations contained identical acoustic features except reversed temporal information (**Supplementary Fig. 3B, C**). Note that temporally reversed vocalizations were employed here as the control for forward (i.e., true and behaviorally relevant) vocalizations. Such temporally reversed vocalizations exhibited the identical sound pressure level (SPL that is important to BOLD response level), but triggered minimal behavioral responses (Gao et al., 2015).

In the control experiment, broadband noise (bandwidth: 1 – 40 kHz; SPL: 83 dB) was presented to the left/contralateral ear canal of the animals in a standard block-design paradigm (40 seconds sound-off followed by four blocks of 20 seconds sound-on and 40 seconds sound-off, fMRI no. of time points = 280) (**Supplementary Fig. 4A**). During each 20 seconds sound-on period, the broadband noise was presented with amplitude modulation at 4 Hz and 80 % duty cycle (**Supplementary Fig. 4B**).

2.5. Tetrodotoxin (TTX) Infusion and Auditory fMRI Experiment

Before animals were placed in the magnet, surgery was performed to implant an MRI-compatible cannula, 250-μm internal diameter in vHP (**Supplementary Fig. 5A**). A total of sixteen auditory fMRI sessions were performed in each animal (**Supplementary Fig. 5B**). After eight sessions, 5 μL TTX (concentration: 5-10 ng/μL) (Chan et al., 2017, Telensky et al., 2011) was infused into vHP. The next immediate session was then acquired one minute after the TTX infusion. During auditory fMRI sessions, auditory stimuli were presented to the left/contralateral ear canal of the animals. Aversive vocalization and its temporal reversion (i.e., identical to the one used for combined optogenetic and auditory fMRI experiment in **Supplementary Fig. 3B**) were presented in standard block design paradigm (40 s sound-off followed by 4 blocks of 20 s sound-on and 40 s sound-off, fMRI no. of time points = 280). Auditory fMRI sessions were interleaved (i.e., either starting with forward aversive vocalization or temporally reversed aversive vocalization) (**Supplementary Fig. 5B**).

2.6. MRI Acquisitions

Twelve coronal slices with 1.0 mm thickness were positioned to cover the ascending auditory pathway with the 2^{nd,} and 3rd slice covered the whole IC. T2-weighted images were acquired as anatomical reference using a Rapid Acquisition with Refocused Echoes (RARE) sequence (FOV = 32×32 mm^2, data matrix = 256×256, RARE factor = 8,

echo time (TE) = 36, repetition time (TR) = 4200 ms). All fMRI measurements were obtained using a multi-slice single-shot Gradient-Echo Echo-Planar-Imaging (GE-EPI) sequence (FOV = 32×32 mm^2, data matrix = 64×64, flip angle = 56°, TE/TR = 20/1000 ms, temporal resolution = 1000ms).

2.7. fMRI Data Analysis

For each animal, the fMRI images were realigned to the mean image of the first fMRI session (SPM12, Wellcome Department of Imaging Neuroscience, University College London, UK). FMRI sessions suffering from motion artifacts (>0.125 mm voxel shifts detected by realignment) and sudden physiological changes (i.e., abrupt changes in respiration pattern, heart rate and oxygen saturation level) were discarded. Images from each animal were co-registered to a custom-made brain template using affine transformation and Gaussian smoothing, with the criteria of maximizing normalized mutual information (SPM12). For optogenetic fMRI and auditory fMRI, data from repeated sessions were averaged, in-plane smoothed (FWHM = 1 pixel), and high-pass filtered (128 s), and then standard general linear model (GLM) was applied, to calculate the BOLD response coefficient (β) maps for each auditory stimulus (SPM12). Hence, activation at the optogenetically stimulated region, vHP, was not observed in the optogenetic fMRI and auditory fMRI experiments due to the continuous 5 Hz stimulation paradigm. Typically, in each animal, three fMRI sessions were averaged for each stimulation frequency in the vHP optogenetic stimulation only experiments, whereas four sessions were averaged for combined auditory and vHP optogenetic stimulation. Finally, activated voxels were identified with Student's t-test on the β values ($p < 0.01$).

The regions-of-interests (ROIs) were defined by identifying clusters of activated voxels ($p < 0.05$) that were restricted within the anatomical location of each region. Anatomical locations of each identified region were determined using the Paxinos & Watson rat brain atlas. In individual animals, the BOLD signal profiles for each ROI were first extracted and averaged across voxels, before they were separated into six blocks (each covering a period from 10 s before to 30 s after a sound-on period) and two blocks (each covering a period from 10 s before to 50 s after an optogenetic-ON period for optogenetic stimulation only experiments), respectively. They were then averaged across stimulation blocks and normalized by the mean signal intensity of the first 10 s to calculate the percentage of BOLD signal change. Final averaging was then performed across animals to generate BOLD signal profiles. Given the relatively large size of the inferior colliculus (IC) compared to the medial geniculate nucleus (MGB), or auditory cortex (AC), three additional ROIs covering different IC subdivisions were defined as in our previous auditory fMRI study (Gao et al., 2015, Gao et al., 2015). Note that the size of ROI for each IC subdivision was different, and this could influence the absolute SNR of the averaged BOLD responses.

In individual animals, β values were also extracted from each ROI and averaged across voxels. The final β value used for comparison between the BOLD responses to the sound stimulus with and without optogenetic stimulation of the vHP was computed by averaging. Further, the β value difference between forward and reversed vocalizations ($\beta_{Forward} - \beta_{Reversed}$), as a metric of response selectivity, was compared between with and without optogenetic stimulation.

3. Results

3.1. Brain-wide propagation of neural activity initiated at ventral hippocampus

We characterized the downstream targets of vHP using optogenetics to selectively stimulate CaMKIIα-expressing vHP excitatory neurons, primarily in the dentate gyrus of vHP in the right/ipsilateral brain hemisphere. Anatomical MRI scans confirmed the location of the virus injection and optical fiber implantation in vHP of all animals (Fig. 1A). Immunohistochemistry confirmed that CaMKIIα^+ excitatory neurons of the vHP (Fig. 1B), but not GABAergic inhibitory neurons, expressed ChR2-mCherry (**Supplementary Fig. 1A**).

To examine frequency-dependent spatiotemporal characteristics of brain-wide, long-range evoked BOLD responses driven by vHP, we performed whole-brain optogenetic fMRI in lightly anesthetized rats (i.e., 1.0% isoflurane). Blue light pulses at five frequencies (1 Hz with 10 % duty cycle, 5 Hz, 10 Hz, 20 Hz, and 40 Hz with 30 % duty cycle; light intensity, 40 mW/mm^2) were delivered to vHP neurons in a block design paradigm (**Supplementary Fig. 2A**). We chose a reduced duty cycle for 1 Hz stimulation to avoid excessively long stimulation pulse width that may not be physiological. 5 Hz optogenetic stimulation of vHP evoked robust brain-wide positive BOLD activations in regions related to learning, memory, sensory processing and emotion, including bilateral vHP, dorsal hippocampus (dHP), entorhinal cortex (Ent), primary auditory cortex (AC), perirhinal cortex (Prh), amygdala (AMG), medial septum (MS), lateral septum (LS), diagonal band of Broca (DBB), and cingulate cortex (Cg) (Fig. 2). Note that we did not detect any positive BOLD activations in IC and MGB in midbrain and thalamus, respectively. Such brain-wide activations evoked by 5 Hz stimulation indicated a high possibility of sound processing modulation. Importantly, we found robust BOLD activations in the AC only during 5 Hz stimulation at vHP, but not at the other four frequencies (1 Hz, 10 Hz, 20 Hz, 40 Hz) (**Supplementary Fig. 2C**). These frequencies evoked weaker BOLD responses in Prh, MS, and LS, and Cg, while retaining strong BOLD responses in vHP and dHP. Altogether, these results demonstrate the most extensive brain-wide vHP downstream targets found at 5 Hz stimulation, especially the robust BOLD activations in AC. These findings indicate that 5 Hz vHP stimulation generates strong and robust hippocampal activity outputs to AC and other regions, likely modulating sound processing brain-wide.

3.2. Hippocampal outputs enhance neural responses and their selectivity to vocalizations with negative valence in auditory midbrain, thalamus and cortex

To explore the large-scale hippocampal modulatory effects on early auditory processing of natural sound (i.e., vocalizations), we performed auditory fMRI with and without continuous 5 Hz optogenetic stimulation at vHP. Forward aversive vocalizations (i.e., natural and behaviorally relevant) and the same but temporally reversed vocalizations (i.e., artificial and behaviorally irrelevant) were presented to the left/contralateral ear in a block-design paradigm (**Supplementary Fig. 3A**). As expected, auditory evoked BOLD responses occurred along the ascending auditory pathway in the right/ipsilateral brain hemisphere, including ipsilateral IC, MGB, and bilateral AC (Fig. 3). Without optogenetic stimulation, the BOLD responses (as described by β values) in IC, MGB and AC were stronger using forward than reversed vocalizations (with β percentage difference between forward and reversed vocalization responses in IC: 8.6 ± 2.7 %, $p < 0.01$; MGB: 34.7 ± 10.53 %, $p < 0.05$; AC: 22.0 ± 7.7 %, $p < 0.05$, paired Student's t-test followed by Holm-Bonferroni correction). This finding demonstrates the response selectivity to forward vocalizations, which is consistent with our prior findings in rodent auditory system (Gao et al., 2015). Here, the response selectivity was most prominent in the external cortex (ECIC) and dorsal cortex (DCIC) of IC (with β percentage difference in ECIC: 8.8 ± 2.6 %, $p < 0.01$; DCIC: 7.8 ± 1.6 %, $p < 0.01$, paired Student's t-test followed by Holm-Bonferroni correction).

Optogenetic 5 Hz vHP stimulation significantly enhanced response selectivity to forward vocalizations throughout the ascending auditory pathway (with the β percentage difference between forward and reversed vocalization responses in IC: 16.3 ± 3.5 %, $p < 0.01$; MGB: 166.2 ± 57.6 %, $p < 0.01$; AC: 46.5 ± 11.9 %, $p < 0.001$, paired Student's t-test followed by Holm-Bonferroni correction). Specifically, only the BOLD responses in IC, MGB and AC evoked by the forward vocalizations were significantly increased by optogenetic stimulation (with β

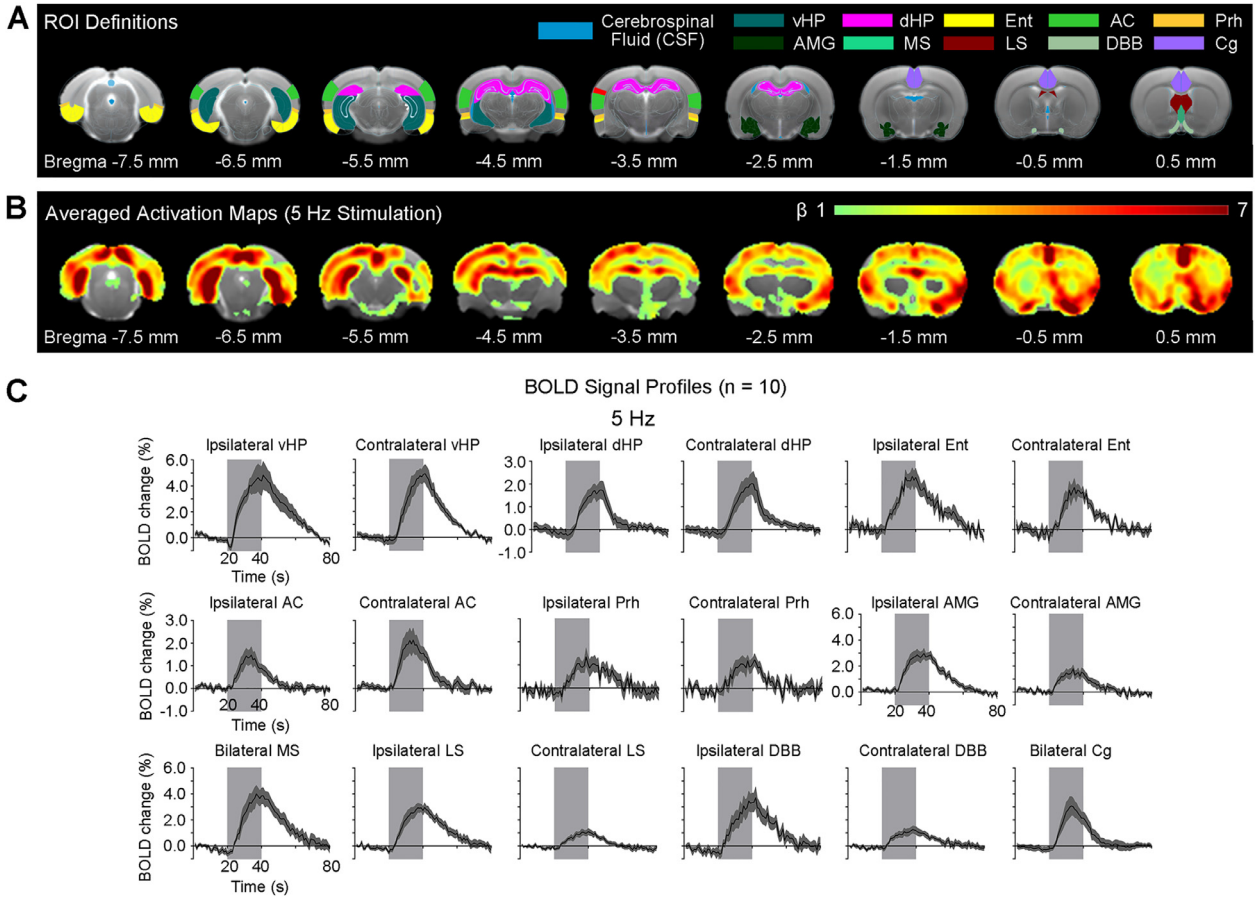

Fig. 2. Brain-wide activations detected in the hippocampal formation, and cortical and subcortical regions during 5 Hz optogenetic stimulation of excitatory neurons in vHP. ***(A)*** Regions of interest (ROIs) defined by the rat brain atlas used to extract the BOLD signal profiles. ***(B)*** Averaged activation (β) maps of optogenetic stimulation in vHP. Robust positive BOLD responses detected in bilateral vHP, dHP, Ent, AC, Prh, AMG, MS, LS, DBB, and Cg during 5 Hz optogenetic stimulation (n = 10; t > 3.1; corresponding to $p < 0.001$). ***(C)*** BOLD signal profiles extracted from the ROIs. Error bars indicate ± SEM. The area shaded in grey indicates the 20 s 5 Hz optogenetic stimulation window. Abbreviations: Ventral Hippocampus (vHP); Dorsal Hippocampus (dHP); Entorhinal Cortex (Ent); Auditory Cortex (AC); Perirhinal Cortex (Prh); Amygdala (AMG); Medial Septum (MS); Lateral Septum (LS); Diagonal Band of Broca (DBB); Cingulate Cortex (Cg).

percentage increase in forward vocalization response in IC: 18.2 ± 7.3 %, $p < 0.05$; MGB: 76.5 ± 22.6 %, $p < 0.01$; AC: 28.7 ± 14.1 %, $p < 0.05$, paired Student's t-test followed by Holm-Bonferroni correction). This finding demonstrates that the hippocampal outputs modulate the responses to forward vocalizations that convey contextual information. Note that such increased responses in IC occurred in ECIC and DCIC, as well as CNIC (with β increase in ECIC: 20.5 ± 9.5%, $p < 0.05$; DCIC: 20.8 ± 4.2 %, $p < 0.001$, CNIC: 26.3 ± 6.1 %, $p < 0.01$, paired Student's t-test followed by Holm-Bonferroni correction). Note that we did not observe robust responses to the aversive vocalization sound in the hippocampus likely due to the limited sensitivity of BOLD fMRI in detecting weak hippocampal neural activity in response to sound from a localized small neural population (Xiao et al., 2018, Rothschild et al., 2017, Mays and Best, 1975). Altogether our fMRI results indicate that hippocampal outputs (initiated by the 5 Hz vHP stimulation) can enhance IC, MGB and AC auditory responses and their selectivity to behaviorally relevant sounds at early processing centers within the ascending auditory pathway.

3.3. Hippocampal outputs enhance neural responses and their selectivity to vocalizations with positive valence

We then utilized the same approach to examine whether such hippocampal modulation on vocalizations was biased for only the aversive content. So, we performed auditory fMRI with postejaculatory vocalizations with and without presenting the 5 Hz optogenetic stimulation at vHP. Similarly, auditory evoked BOLD responses predominantly occurred along the ipsilateral ascending auditory pathway, including IC, MGB, and AC (Fig. 4). Without optogenetic stimulation, the BOLD responses evoked by postejaculatory vocalizations also showed response selectivity to the forward one (with β percentage difference between forward and reversed vocalization responses in IC: 7.8 ± 1.7 %, $p < 0.001$; MGB: 43.0 ± 16.2 %, $p < 0.05$; AC: 40.5 ± 14.4 %, $p < 0.05$, paired Student's t-test followed by Holm-Bonferroni correction). Consistent with the results of aversive vocalization experiment, the response selectivity to forward postejaculatory vocalizations in IC was mainly observed in ECIC and DCIC (with β percentage difference in ECIC: 5.4 ± 1.8 %, $p < 0.01$; DCIC: 6.5 ± 2.5 %, $p < 0.05$, paired Student's t-test followed by Holm-Bonferroni correction), but not CNIC (no significant difference).

During optogenetic stimulation, similar to the aversive vocalization experiment, the response selectivity to the forward postejaculatory vocalizations was significantly enhanced throughout the ascending auditory pathway (with the β percentage difference between forward and reversed vocalization responses in IC: 19.2 ± 3.5 %, $p < 0.001$; MGB: 118.1 ± 43.0 %, $p < 0.01$; AC: 84.7 ± 23.2 %, $p < 0.001$, paired Student's t-test followed by Holm-Bonferroni correction). Specifically, such enhancement primarily arose from increased responses to forward vocalizations (with β percentage increase in forward vocalization response

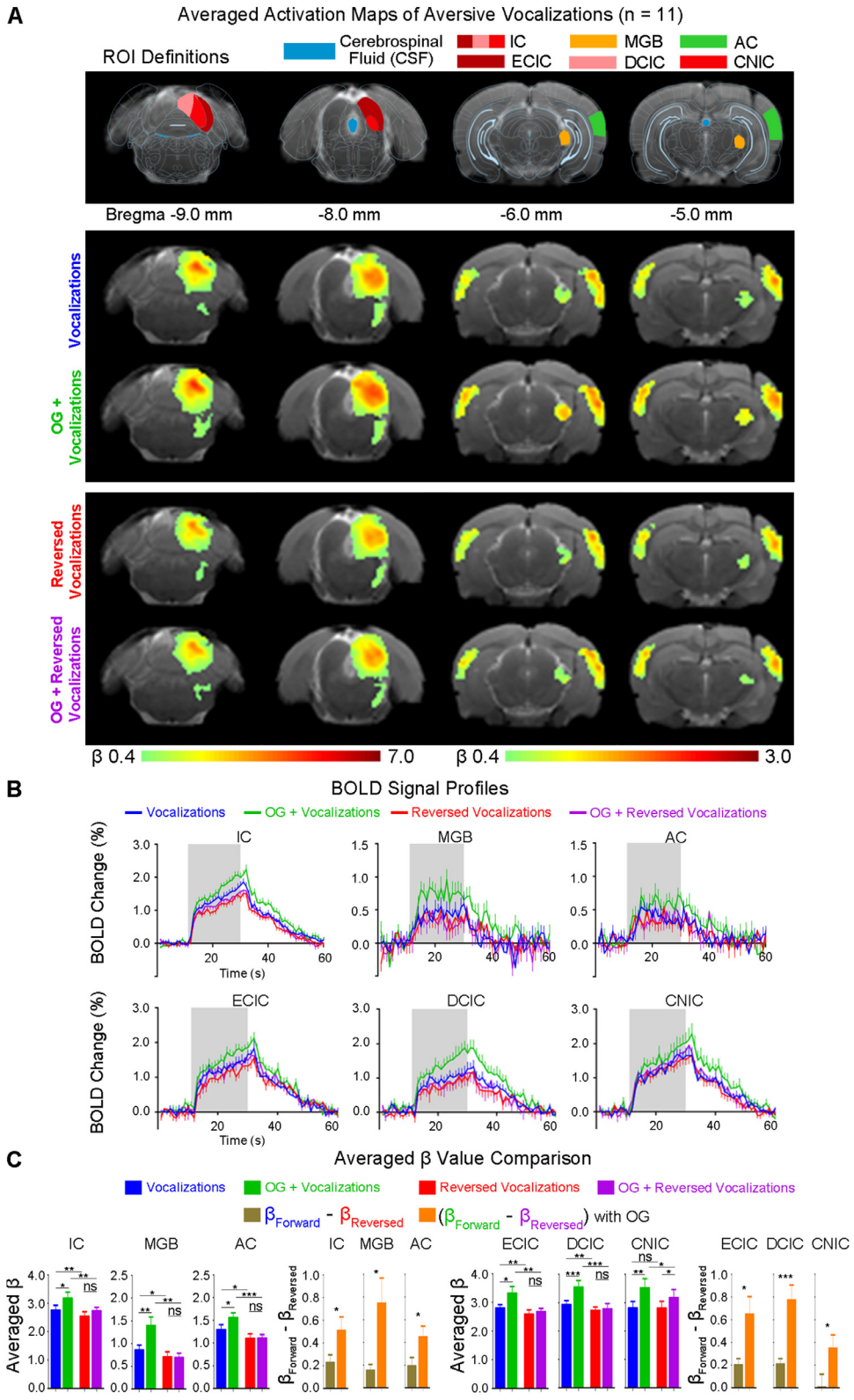

Fig. 3. vHP optogenetic stimulation enhances neural responses and their selectivity to aversive vocalizations in the auditory midbrain (inferior colliculus or IC), thalamus (medial geniculate body or MGB), and cortex (auditory cortex or AC). ***(A)*** Illustration of the atlas-based region of interest (ROI) definitions *(Top)*. Averaged BOLD activation (β) maps with and without 5-Hz optogenetic (OG) stimulation generated by fitting a canonical hemodynamic response function (HRF) to individual voxels in the fMRI image (n = 11; $t > 2.6$; corresponding to $p < 0.01$) *(Bottom)*. Note that two color bar ranges with differing upper bound β values were used to visualize responses in the IC (Bregma -9.0 and -8.0 mm) and MGB/AC (Bregma -6.0 and -5.0 mm), respectively, due to the two-fold difference in peak BOLD amplitudes as shown in *B*. ***(B)*** BOLD signal profiles extracted from the corresponding ROIs (IC, MGB, AC, ECIC, DCIC, and CNIC). Error bars indicate ± SEM. The area shaded in grey indicates the 20 s acoustic stimulation. ***(C)*** BOLD signal (averaged β) comparison showing the modulatory effects of optogenetic stimulation on responses to forward aversive vocalizations in IC, MGB, AC, ECIC, DCIC, and CNIC, but not temporally reversed counterparts (that are artificial and evoke no behavioral response). Statistical comparisons were performed using paired two-sample t-test followed by Holm-Bonferroni correction with * for $p < 0.05$, ** for $p < 0.01$, *** for $p < 0.001$, and n.s. for not significant.

in IC: 15.2 ± 4.8 %, $p < 0.01$, MGB: 123.1 ± 36.6%, $p < 0.01$; AC: 74.7 ± 34.2 %, $p < 0.05$, paired Student's t-test followed by Holm-Bonferroni correction). In IC, such increased responses were found in ECIC, DCIC as well as CNIC (with β increase in ECIC: 16.0 ± 6.3 %, $p < 0.05$; DCIC: 9.8 ± 3.0 %, $p < 0.01$; CNIC: 17.3 ± 4.3 %, $p < 0.01$, paired Student's t-test followed by Holm-Bonferroni correction). Taken together, these results demonstrate that the hippocampus plays a key role in modulating natural vocalization processing. Such hippocampal modulatory effects are not biased towards the aversive content embedded in the vocalizations.

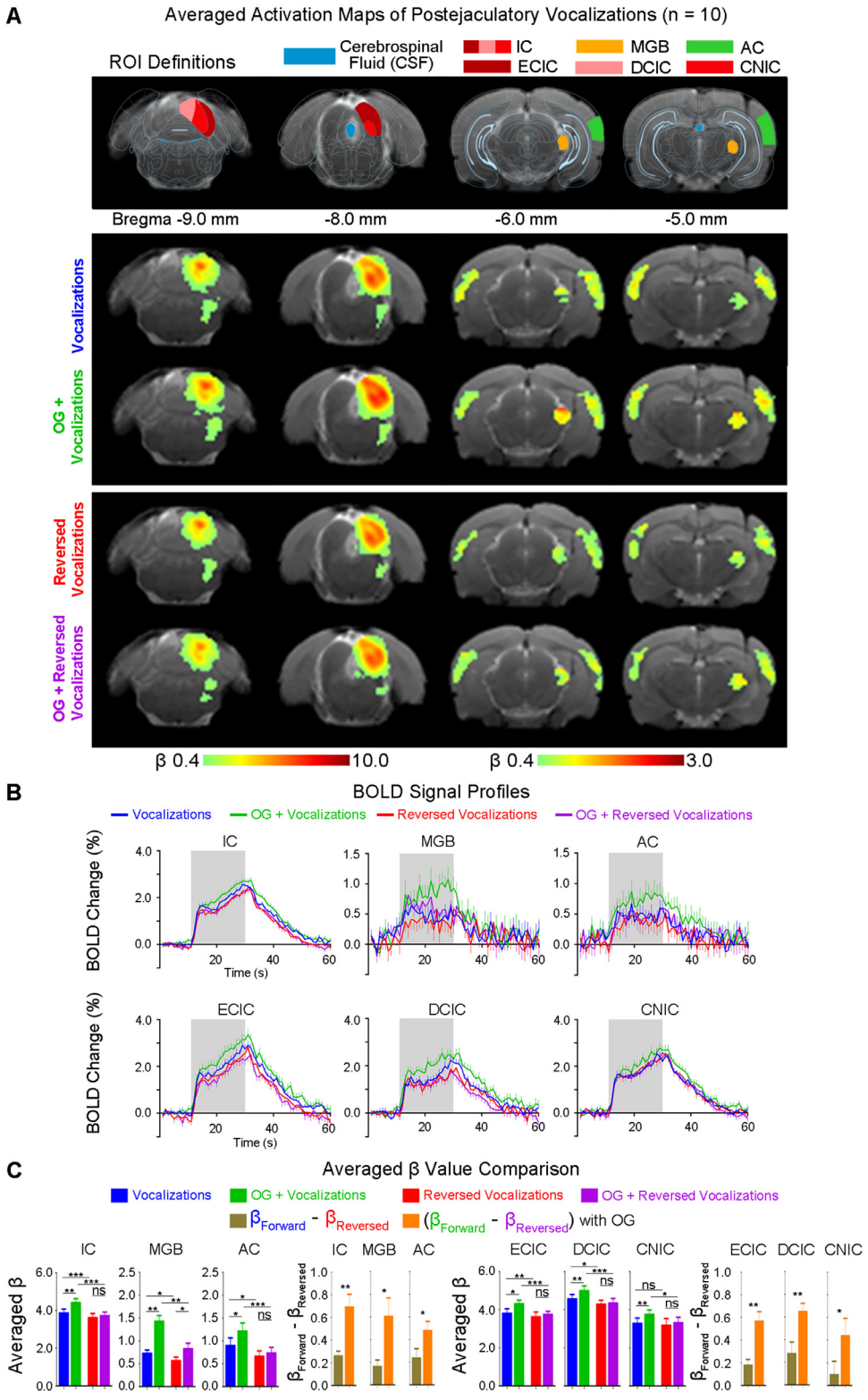

Fig. 4. vHP optogenetic stimulation enhances neural responses and their selectivity to postejaculatory vocalizations in the auditory midbrain (IC), thalamus (MGB), and cortex (AC). ***(A)*** Illustration of the atlas-based region of interest (ROI) definitions *(Top)*. Averaged BOLD activation (β) maps with and without 5-Hz optogenetic stimulation *(Bottom)* generated by fitting a canonical HRF to individual voxels in the fMRI image (n = 10; $t > 2.6$; corresponding to $p < 0.01$). ***(B)*** BOLD signal profiles extracted from the corresponding ROIs (IC, MGB, AC, ECIC, DCIC, and CNIC). Error bars indicate ± SEM. The area shaded in grey indicates 20 s acoustic stimulation. ***(C)*** BOLD signal (averaged β) comparison showing the modulatory effects of optogenetic stimulation on responses to forward postejaculatory vocalizations in IC, MGB, AC, ECIC, DCIC, and CNIC, but not the temporally reversed counterparts. Statistical comparisons were performed using paired two-sample t-test followed by Holm-Bonferroni correction with * for $p < 0.05$, ** for $p < 0.01$, *** for $p < 0.001$, and n.s. for not significant.

3.4. Hippocampal outputs do not overtly alter neural responses to broadband acoustic noise

To further investigate whether the modulatory effects of hippocampal outputs are only specific to auditory processing of behaviorally relevant sounds, we replaced the vocalizations with a basic acoustic stimulus, 1 – 40 kHz broadband noise (**Supplementary Fig. 4**). As expected, the broadband noise evoked BOLD responses primarily along the ipsilateral ascending auditory pathway, including IC, MGB, and AC. Importantly, the noise evoked BOLD responses in IC, MGB, and AC remained unchanged during the vHP stimulation (Fig. 5). This finding reveals that the hippocampal outputs do not overtly influence behaviorally irrelevant or basic acoustic stimuli.

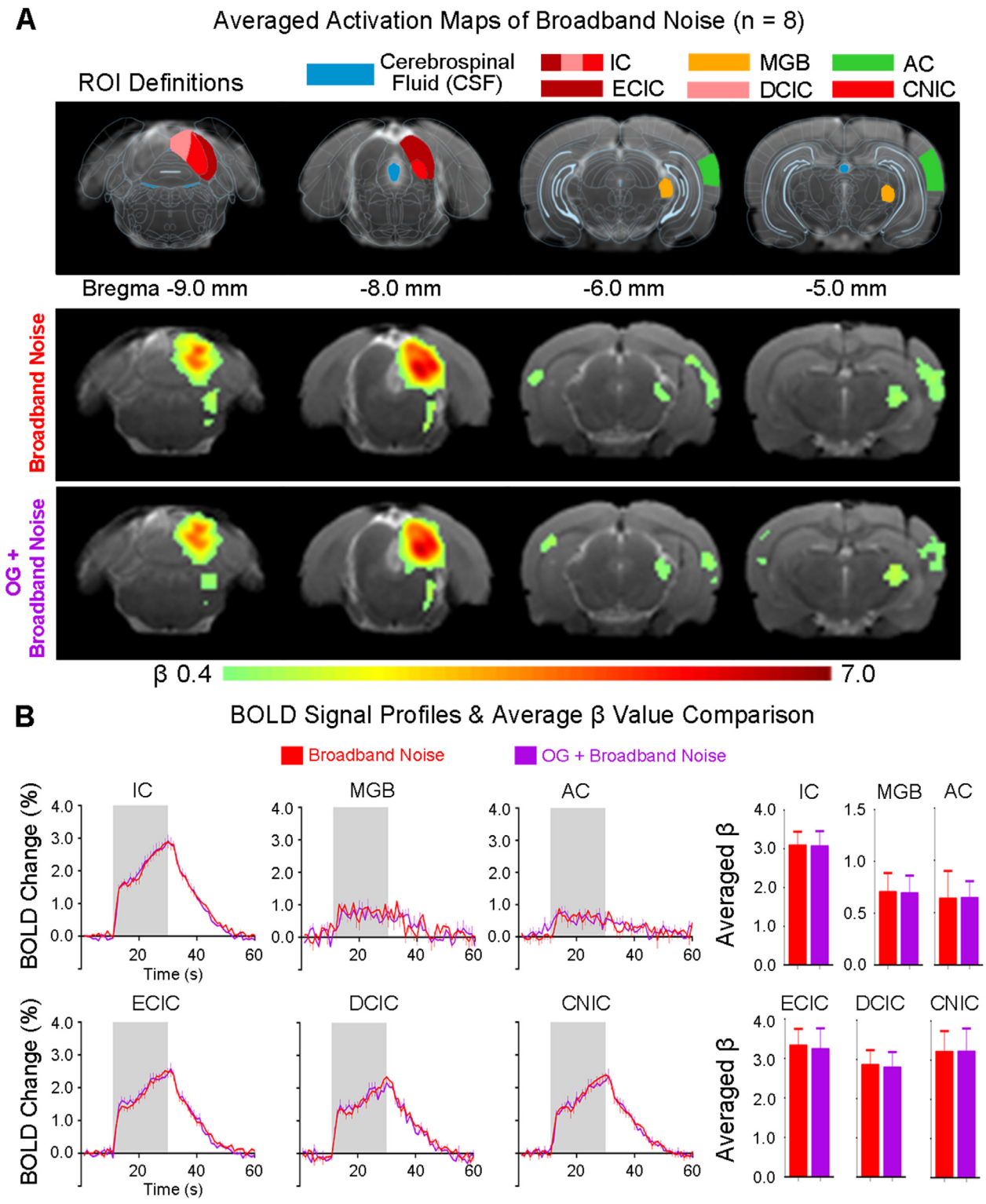

Fig. 5. vHP optogenetic stimulation shows no modulatory effects on the responses to broadband acoustic noise in the auditory midbrain (IC), thalamus (MGB), and cortex (AC). ***(A)*** Illustration of the atlas-based region of interest (ROI) definitions *(Top)*. Averaged BOLD activation (β) maps with, without 5-Hz optogenetic stimulation *(Bottom)* generated by fitting a canonical HRF to individual voxels in the fMRI image (n = 8; t > 2.6; corresponding to $p < 0.01$). ***(B)*** BOLD signal profiles *(Left)* extracted from the corresponding ROIs (IC, MGB, AC, ECIC, DCIC, and CNIC). Error bars indicate ± SEM. The area shaded in grey indicates the 20 s acoustic stimulation. BOLD signal (averaged β) comparison *(Right)* showing no effects of optogenetic stimulation on broadband noise responses in IC, MGB, and AC. Statistical comparisons were performed using paired two-sample t-test followed by Holm-Bonferroni correction.

3.5. Pharmacological hippocampal inactivation alters auditory responses and their selectivity for vocalizations

In addition, we examined the effects of pharmacologically inactivating neurons in the dentate gyrus of vHP on vocalization sound processing using TTX. Auditory fMRI was performed before (PRE) and after (POST) infusion of TTX at vHP (**Supplementary Fig. 5**). As expected, before the TTX infusion, the BOLD responses evoked by aversive vocalizations showed response selectivity to the forward one (Fig. 6) (with β percentage difference between forward and reversed vocalization responses in IC: 15.6 ± 1.9 %, $p < 0.01$; MGB: 77.6 ± 23.5 %, $p < 0.05$; AC: 132.2 ± 60.5 %, $p < 0.05$, paired Student's t-test followed by Holm-Bonferroni correction). Similarly, the response selectivity to forward aversive vocalizations in IC was mainly observed in ECIC and DCIC (with β percentage difference in ECIC: 11.2 ± 4.1 %, $p < 0.05$; DCIC: 31.4 ± 8.8 %, $p < 0.05$, paired Student's t-test followed by Holm-Bonferroni correction), but not in CNIC.

Notably, pharmacological vHP inactivation via TTX infusion abolished the response selectivity to forward aversive vocalizations throughout the ascending auditory pathway, including IC, MGB, and AC. In general, the BOLD responses to forward and reversed vocalizations were also reduced. Yet the BOLD responses to forward vocalizations were diminished by a much greater extent (with β percentage decrease in forward vocalization response in IC: -20.6 ± 3.9 %, $p < 0.01$; MGB: -54.4 ± 21.5 %, $p < 0.05$; AC: -44.9 ± 17.0 %, $p < 0.05$, paired Student's t-test followed by Holm-Bonferroni correction). In IC, such decreased responses were mainly found in ECIC and DCIC (with β percentage decrease in ECIC: -12.9 ± 3.9 %, $p < 0.05$; DCIC: -18.3 ± 3.6 %, $p < 0.01$, paired Student's t-test followed by Holm-Bonferroni correction), but not in CNIC. These findings present additional evidence that vHP modulates and shapes IC, MGB and AC response selectivity to behaviorally relevant sounds at early sound processing centers within the ascending auditory pathway.

4. Discussion

In the classical view, the auditory cortex processes complex auditory features and provides corticofugal feedback to modulate the responses in IC and MGB (Chechik et al., 2006, Zhang et al., 2018, Aronov et al., 2017, Guo et al., 2019, Xiao et al., 2018). In particular, the existing hierarchical notion of cortical processing (Rauschecker and Scott, 2009, Rauschecker and Tian, 2000, Guo et al., 2017) postulates that the AC decodes the spectrotemporal dynamic features of auditory inputs, which facilitate responses to complex natural acoustic stimuli like vocalizations (Leaver and Rauschecker, 2010). However, studies suggest that complex sound processing may also occur at early auditory centers (Mihai et al., 2019, Diaz et al., 2012). Converging evidence indicates that extraction and processing of spectral and temporal features begin at the midbrain level for discriminating natural sounds (Felix et al., 2018, Winer and Schreiner, 2005), such as vocalizations (Gao et al., 2015, Pollak, 2013, Woolley and Portfors, 2013). Moreover, an electrophysiological study showed that IC and MGB represent more comprehensive stimulus identities of natural stimuli relative to the cortex (Chechik et al., 2006), highlighting the importance of early auditory structures in processing natural sounds. In addition, recent discoveries of non-canonical regions in processing complex auditory stimuli, such as Ent and MS (Zhang et al., 2018, Aronov et al., 2017), and inevitably the hippocampus due to the dense reciprocal axonal projections (Oh et al., 2014, Muller and Remy, 2018), challenge current dogma on the hierarchical notion of cortical processing.

Here, we experimentally revealed that the hippocampus, a limbic region vital for learning and memory functions, modulates auditory responses to natural sound processing along the early ascending auditory pathway by monitoring auditory responses during optogenetic vHP stimulation or pharmacological inactivation using large-view fMRI. We discovered a robust hippocampal influence on BOLD responses to vocalizations, but not artificial/basic acoustic stimuli, in the auditory midbrain, thalamus, and cortex. However, due to the limited sensitivity of fMRI, we do not discount the weak neural activity changes in small neural populations in response to artificial/basic acoustic stimuli at IC, MGB and AC that can be caused by vHP outputs. Nevertheless, these fMRI results directly support the large-scale and faciliatory influence of the hippocampus on vocalization sound processing and shaping the corresponding response selectivity in early auditory centers within the ascending auditory pathway.

4.1. Hippocampal outputs enhance responses to vocalizations at early auditory centers and the pathways likely subserving such hippocampal top-down modulation

The exact mechanisms underlying our experimentally observed selective modulation of vocalizations by optogenetically triggered hippocampal outputs remains unclear and requires further investigation. We posit that specific spectrotemporal information embedded in the sound drive this specificity. The hippocampus is positioned to process temporal information of sensory inputs (Aronov et al., 2017, Eichenbaum, 2014), as hippocampal lesions can impair memory for the temporal order of events in both animals (Kesner et al., 2005, DeVito et al., 2009) and humans (Mayes et al., 2001, Spiers et al., 2001). When learning to associate specific time intervals with a given stimulus, the hippocampus is essential for discriminating minute temporal differences in rodents (Jacobs et al., 2013). These findings indicate that the hippocampus plays a critical role in encoding and recognizing temporal information to subsequently discriminate and interpret the temporal organization of incoming sensory inputs. We observed that hippocampal modulation primarily facilitates auditory responses in IC, MGB, and AC to both types of vocalizations (i.e., aversive/fear and postejaculatory/positive), but not their temporally reversed counterparts (Figs. 3 and 4). Moreover, blocking hippocampal outputs through pharmacological manipulation altered responses to forward vocalizations, and consequently disrupted the response selectivity to vocalizations (Fig. 6). We postulate that temporally reversing vocalizations alter specific properties. Reversed vocalizations no longer carry the critical information embedded in forward vocalizations, which diminishes the behavioral relevance of the sound. The hippocampus, by interpreting and discriminating the embedded spectrotemporal features of the incoming sounds, can discriminate and recognize behaviorally relevant stimuli by contextual memory recall according to past experience (Tanaka et al., 2018, Ross et al., 2018) and then can exert selective influence to downstream targets.

Multiple complementary pathways likely subserve long-range hippocampal modulation of central auditory processing of vocalizations (Fig. 7). Recent evidence indicates that the reticular limbic auditory pathway may provide a fast route to relay auditory inputs from the cochlear nucleus to high-order regions (Zhang et al., 2018), suggesting that the hippocampus receives and processes behaviorally relevant auditory inputs via Ent and MS. Further, our histological findings showed strong anterograde ChR2 mCherry expression in the MS and LS, as well as the DBB (**Supplementary Fig. 1B**), suggesting a circuit loop that is dedicated for auditory processing outside of the central pathways. These regions support learning (Vega-Flores et al., 2014) and memory functions (Klinkenberg and Blokland, 2010), particularly related to auditory processes. For instance, MS inactivation impairs acquiring auditory fear memory (Xiao et al., 2018). MS and DBB are the primary sources of cholinergic projections to HP and AMG (Chavez and Zaborszky, 2017), which can be critical for contextual memory formation (Tronson et al., 2009), sensory cue detection and discrimination (Gritton et al., 2016, Roland et al., 2014). Disrupting MS and DBB cholinergic projections to vHP prevents auditory fear memory acquisition and retention (Staib et al., 2018). Further, a prior study showed that systemic blockade of cholinergic signaling via atropine, a muscarinic acetylcholine receptor antagonist, inhibited response selectivity to vo-

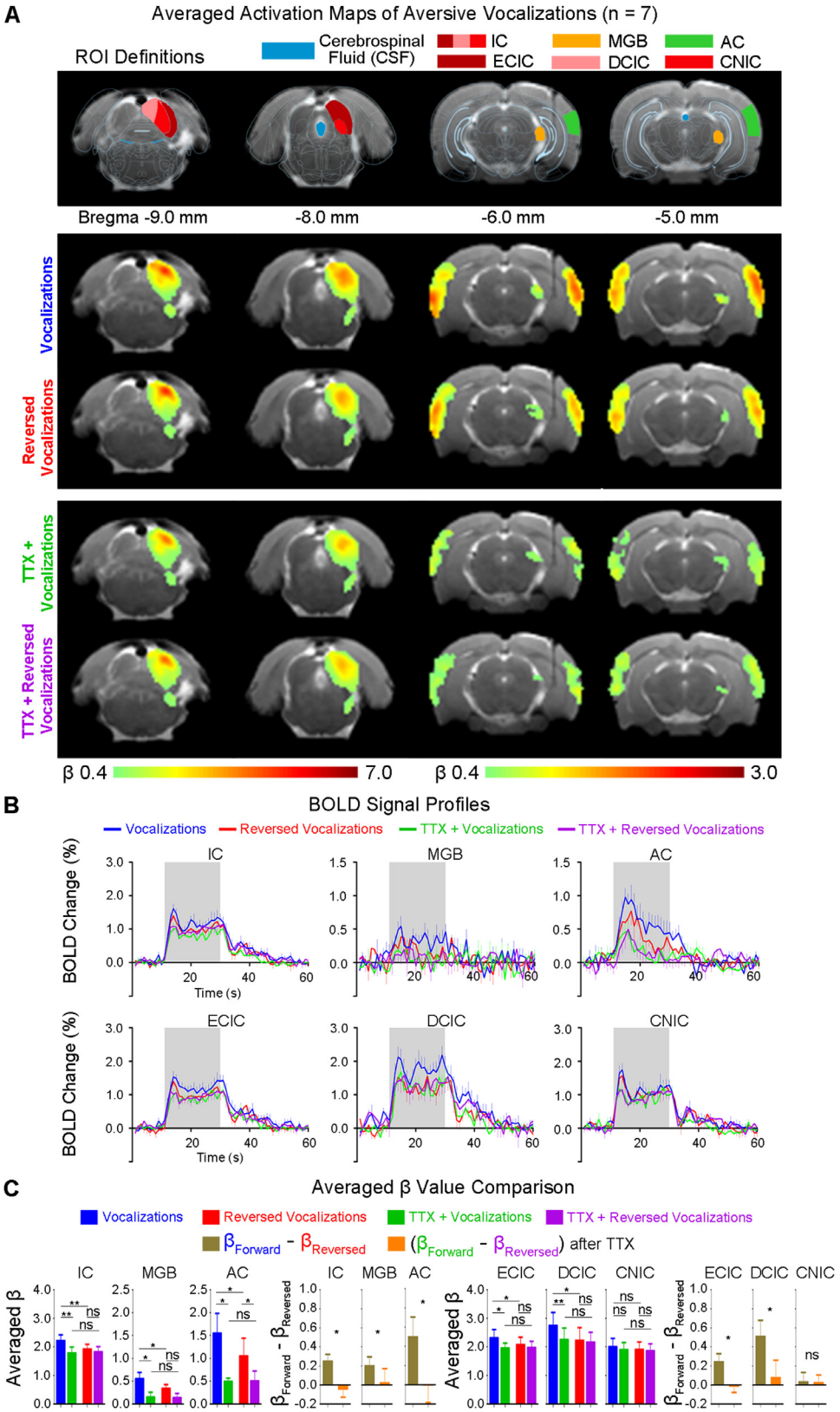

Fig. 6. Pharmacologically inactivating vHP alters neural responses and decreases their selectivity to aversive vocalizations in the auditory midbrain (IC), thalamus (MGB), and cortex (AC). ***(A)*** Illustration of the atlas-based region of interest (ROI) definition *(Top)*. Averaged BOLD activation (β) maps before and after TTX infusion *(Bottom)* generated by fitting a canonical hemodynamic response function (HRF) to individual voxels in the fMRI image (n = 7; t > 2.6; corresponding to $p < 0.01$). ***(B)*** BOLD signal profiles extracted from the corresponding ROIs (IC, MGB, AC, ECIC, DCIC, and CNIC). Error bars indicate ± SEM. The area shaded in grey indicates 20 s acoustic stimulation. ***(C)*** BOLD signal (averaged β) comparison showing the effects of TTX inactivation of vHP neurons predominantly on responses to forward aversive vocalizations in IC, MGB, AC, ECIC, and DCIC. Statistical comparisons were performed using paired two-sample t-test followed by Holm-Bonferroni correction with * for $p < 0.05$, ** for $p < 0.01$, *** for $p < 0.001$, and n.s. for not significant.

calizations in the auditory midbrain (Gao et al., 2015). Here, robust activations in the septum complex (i.e., MS, LS, and DBB) initiated from vHP (Fig. 2B, C) may trigger rapid downstream signaling cascades in the cholinergic system (Gritton et al., 2016) and evoke postsynaptic responses at the terminal fields (Nelson and Mooney, 2016), such as the AMG. Cholinergic signaling within AMG is crucial for encoding and processing emotionally salient memories (Jiang et al., 2016), which could facilitate selective amplification of auditory responses evoked by behaviorally relevant stimuli. Overall, we detected robust activations in cortical (i.e., AC, Ent, Prh, Cg) and subcortical regions (i.e., AMG, MS, LS, DBB) during 5 Hz optogenetic stimulation at vHP (Fig. 2B, C). The hippocampal modulatory outputs evoked from vHP could propagate and

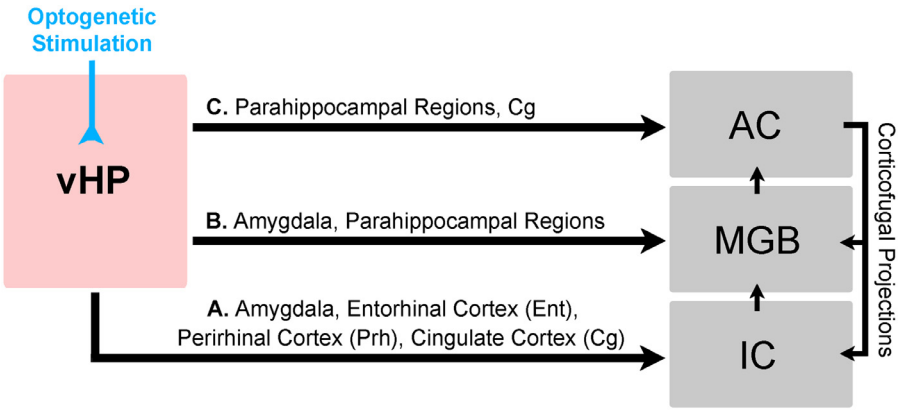

Fig. 7. Schematic pathways of long-range hippocampal modulation of natural sound processing within the ascending auditory pathway through optogenetically-evoked vHP activity. ***Route A:*** vHP could modulate responses in IC via indirect projections from amygdala, entorhinal cortex (Ent), perirhinal cortex (Prh) and cingulate cortex (Cg), which can then enhance the responses in MGB and AC along the ascending auditory pathway. ***Route B:*** vHP can modulate MGB responses indirectly via amygdala and parahippocampal regions, which could subsequently modulate responses in AC via ascending auditory pathway. ***Route C:*** vHP could modulate AC responses directly via hippocampal-cortical projections or indirectly via parahippocampal regions such as Ent, Prh, and Cg via cortico-cortical projections. AC could then modulate the responses in MGB and IC via corticofugal projections.

functionally interact with these activated regions, thereby modulating auditory responses at early auditory centers within the ascending auditory pathway, particularly at the midbrain and thalamic levels.

In this study, we uncovered long-range hippocampal modulation of vocalizations within the ascending auditory pathway during 5 Hz optogenetic stimulation at vHP. However, we do not preclude the potential modulatory effects of other stimulation frequencies like 10 Hz. Even though BOLD activations evoked by 10 Hz optogenetic stimulation were not as widespread as 5 Hz, we still observed robust activations in subcortical regions (e.g., AMG, MS, LS, DBB) albeit with weaker activations in cortical regions (e.g., AC, Prh, Cg) (**Supplementary Fig. 2**). Overall, our findings suggest that hippocampal top-down modulatory outputs, which may be triggered by behaviourally relevant auditory inputs, were augmented by optogenetic stimulation of vHP to enhance responses to vocalizations.

In summary, the present fMRI study established a top-down and large-scale modulatory role for the hippocampus throughout the ascending auditory pathway, including the auditory midbrain, thalamus and cortex, to facilitate natural sound processing such as vocalizations. Our findings expand our present understanding of central auditory system beyond the traditional cortex centric views. Future studies should elucidate the precise hippocampal modulatory processes of natural sound that arise from the brain-wide auditory information processing networks.

Author Contributions

A.T.L.L., E.C.W., and E.X.W. designed research; E.C.W. performed research; A.T.L.L., E.C.W., X.W., and E.X.W. analyzed data; X.W. provided technical assistance; and A.T.L.L., E.C.W., and E.X.W. wrote the paper.

Declaration of Competing Interests

The authors declare no competing financial interests.

Data availability

Data will be made available on request.

Acknowledgments

This work was supported by Hong Kong Research Grant Council (C7048-16G, HKU17112120 and HKU17127121 to E.X. Wu, and HKU17103819 and HKU17104020 to A.T.L. Leong), Lam Woo Foundation, Guangdong Key Technologies for Treatment of Brain Disorders (2018B030332001) and Guangdong Key Technologies for Alzheimer's Disease Diagnostic and Treatment (2018B030336001) to E.X. Wu. We would like to thank Profs. J. He and G. Buzsáki for the insightful scientific discussions. We also thank Drs. R. Chan, C. Dong, A. To, and M. Bialy for their technical assistance. We also thank Dr. K. Deisseroth who provided us with the ChR2 viral construct.

Supplementary materials

Supplementary material associated with this article can be found, in the online version, at doi:10.1016/j.neuroimage.2023.119943.

References

Aronov, D., Nevers, R., Tank, D.W., 2017. Mapping of a non-spatial dimension by the hippocampal-entorhinal circuit. Nature 543, 719–722.
Bendor, D., Wilson, M.A., 2012. Biasing the content of hippocampal replay during sleep. Nat Neurosci 15, 1439–1444.
Bialy, M., Bogacki-Rychlik, W., Kasarello, K., Nikolaev, E., Sajdel-Sulkowska, E.M., 2016. Modulation of 22-khz postejaculatory vocalizations by conditioning to new place: Evidence for expression of a positive emotional state. Behav Neurosci 130, 415–421.
Bird, C.M., Burgess, N., 2008. The hippocampus and memory: insights from spatial processing. Nat Rev Neurosci 9, 182–194.
Blackwell, J.M., Lesicko, A.M., Rao, W., De Biasi, M., Geffen, M.N., 2020. Auditory cortex shapes sound responses in the inferior colliculus. Elife 9.
Buzsaki, G., Moser, E.I., 2013. Memory, navigation and theta rhythm in the hippocampal-entorhinal system. Nat Neurosci 16, 130–138.
Cenquizca, L.A., Swanson, L.W., 2007. Spatial organization of direct hippocampal field CA1 axonal projections to the rest of the cerebral cortex. Brain research reviews 56, 1–26.
Chan, R.W., et al., 2017. Low-frequency hippocampal-cortical activity drives brain-wide resting-state functional MRI connectivity. Proc Natl Acad Sci U S A 114, E6972–E6981.
Chavez, C., Zaborszky, L., 2017. Basal Forebrain Cholinergic-Auditory Cortical Network: Primary Versus Nonprimary Auditory Cortical Areas. Cereb Cortex 27, 2335–2347.
Chechik, G., et al., 2006. Reduction of information redundancy in the ascending auditory pathway. Neuron 51, 359–368.
Chen, L., Wang, X., Ge, S., Xiong, Q., 2019. Medial geniculate body and primary auditory cortex differentially contribute to striatal sound representations. Nat Commun 10, 418.
DeVito, L.M., et al., 2009. Vasopressin 1b receptor knock-out impairs memory for temporal order. J Neurosci 29, 2676–2683.
Diaz, B., Hintz, F., Kiebel, S.J., von Kriegstein, K., 2012. Dysfunction of the auditory thalamus in developmental dyslexia. Proc Natl Acad Sci U S A 109, 13841–13846.
Eggermont, J.J., 2001. Between sound and perception: reviewing the search for a neural code. Hear Res 157, 1–42.
Eichenbaum, H., 2014. Time cells in the hippocampus: a new dimension for mapping memories. Nat Rev Neurosci 15, 732–744.
Fanselow, M.S., Dong, H.W., 2010. Are the dorsal and ventral hippocampus functionally distinct structures? Neuron 65, 7–19.
Felix 2nd, R.A., Gourevitch, B., Portfors, C.V., 2018. Subcortical pathways: Towards a better understanding of auditory disorders. Hear Res 362, 48–60.
Gao, P.P., Zhang, J.W., Fan, S.J., Sanes, D.H., Wu, E.X., 2015. Auditory midbrain processing is differentially modulated by auditory and visual cortices: An auditory fMRI study. Neuroimage 123, 22–32.
Gao, P.P., Zhang, J.W., Chan, R.W., Leong, A.T.L., Wu, E.X., 2015. BOLD fMRI study of ultrahigh frequency encoding in the inferior colliculus. Neuroimage 114, 427–437.
Gritton, H.J., et al., 2016. Cortical cholinergic signaling controls the detection of cues. Proc Natl Acad Sci U S A 113, E1089–E1097.
Guo, W., Clause, A.R., Barth-Maron, A., Polley, D.B., 2017. A Corticothalamic Circuit for Dynamic Switching between Feature Detection and Discrimination. Neuron 95 (180-194), e185.
Guo, W., Robert, B., Polley, D.B., 2019. The Cholinergic Basal Forebrain Links Auditory Stimuli with Delayed Reinforcement to Support Learning. Neuron 103 (1164-1177), e1166.

Jacobs, N.S., Allen, T.A., Nguyen, N., Fortin, N.J., 2013. Critical role of the hippocampus in memory for elapsed time. J Neurosci 33, 13888–13893.
Jiang, L., et al., 2016. Cholinergic Signaling Controls Conditioned Fear Behaviors and Enhances Plasticity of Cortical-Amygdala Circuits. Neuron 90, 1057–1070.
Kesner, R.P., Hunsaker, M.R., Gilbert, P.E., 2005. The role of CA1 in the acquisition of an object-trace-odor paired associate task. Behav Neurosci 119, 781–786.
Kim, G., Doupe, A., 2011. Organized representation of spectrotemporal features in songbird auditory forebrain. J Neurosci 31, 16977–16990.
Klinkenberg, I., Blokland, A., 2010. The validity of scopolamine as a pharmacological model for cognitive impairment: a review of animal behavioral studies. Neurosci Biobehav Rev 34, 1307–1350.
Leaver, A.M., Rauschecker, J.P., 2010. Cortical representation of natural complex sounds: effects of acoustic features and auditory object category. J Neurosci 30, 7604–7612.
Leong, A.T., et al., 2016. Long-range projections coordinate distributed brain-wide neural activity with a specific spatiotemporal profile. Proc Natl Acad Sci U S A 113, E8306–E8315.
Leong, A.T.L., et al., 2018. Optogenetic auditory fMRI reveals the effects of visual cortical inputs on auditory midbrain response. Scientific reports 8, 8736.
Leong, A.T.L., et al., 2019. Optogenetic fMRI interrogation of brain-wide central vestibular pathways. Proc Natl Acad Sci U S A 116, 10122–10129.
Leong, A.T.L., Wang, X., Wong, E.C., Dong, C.M., Wu, E.X., 2021. Neural activity temporal pattern dictates long-range propagation targets. Neuroimage 235, 118032.
Lesicko, A.M.H., Sons, S.K., Llano, D.A., 2020. Circuit Mechanisms Underlying the Segregation and Integration of Parallel Processing Streams in the Inferior Colliculus. J Neurosci 40, 6328–6344.
Lisman, J., et al., 2017. Viewpoints: how the hippocampus contributes to memory, navigation and cognition. Nat Neurosci 20, 1434–1447.
Malmierca, M.S., 2015. Auditory system. In: The rat nervous system. Elsevier, pp. 865–946.
Marsh, R.A., Fuzessery, Z.M., Grose, C.D., Wenstrup, J.J., 2002. Projection to the inferior colliculus from the basal nucleus of the amygdala. J Neurosci 22, 10449–10460.
Mayes, A.R., et al., 2001. Memory for single items, word pairs, and temporal order of different kinds in a patient with selective hippocampal lesions. Cogn Neuropsychol 18, 97–123.
Mays, L.E., Best, P.J., 1975. Hippocampal unit activity to tonal stimuli during arousal from sleep and in awake rats. Exp Neurol 47, 268–279.
Mihai, P.G., et al., 2019. Modulation of tonotopic ventral medial geniculate body is behaviorally relevant for speech recognition. Elife 8.
Muller, C., Remy, S., 2018. Septo-hippocampal interaction. Cell Tissue Res 373, 565–575.
Munoz-Lopez, M.M., Mohedano-Moriano, A., Insausti, R., 2010. Anatomical pathways for auditory memory in primates. Front Neuroanat 4, 129.
Nagel, K.I., Doupe, A.J., 2008. Organizing principles of spectro-temporal encoding in the avian primary auditory area field L. Neuron 58, 938–955.
Nelson, A., Mooney, R., 2016. The Basal Forebrain and Motor Cortex Provide Convergent yet Distinct Movement-Related Inputs to the Auditory Cortex. Neuron 90, 635–648.
Oh, S.W., et al., 2014. A mesoscale connectome of the mouse brain. Nature 508, 207–214.
Ohara, S., Sato, S., Tsutsui, K., Witter, M.P., Iijima, T., 2013. Organization of multisynaptic inputs to the dorsal and ventral dentate gyrus: retrograde trans-synaptic tracing with rabies virus vector in the rat. PLoS One 8, e78928.
Olthof, B.M.J., Rees, A., Gartside, S.E., 2019. Multiple Nonauditory Cortical Regions Innervate the Auditory Midbrain. J Neurosci 39, 8916–8928.
Ono, M., Bishop, D.C., Oliver, D.L., 2017. Identified GABAergic and Glutamatergic Neurons in the Mouse Inferior Colliculus Share Similar Response Properties. J Neurosci 37, 8952–8964.
Overath, T., McDermott, J.H., Zarate, J.M., Poeppel, D., 2015. The cortical analysis of speech-specific temporal structure revealed by responses to sound quilts. Nat Neurosci 18, 903–911.
Pollak, G.D., 2013. The dominant role of inhibition in creating response selectivities for communication calls in the brainstem auditory system. Hear Res 305, 86–101.
Portfors, C.V., 2007. Types and functions of ultrasonic vocalizations in laboratory rats and mice. J Am Assoc Lab Anim Sci 46, 28–34.
Rauschecker, J.P., Scott, S.K., 2009. Maps and streams in the auditory cortex: nonhuman primates illuminate human speech processing. Nat Neurosci 12, 718–724.
Rauschecker, J.P., Tian, B., 2000. Mechanisms and streams for processing of "what" and "where" in auditory cortex. Proc Natl Acad Sci U S A 97, 11800–11806.
Roland, J.J., et al., 2014. Medial septum-diagonal band of Broca (MSDB) GABAergic regulation of hippocampal acetylcholine efflux is dependent on cognitive demands. J Neurosci 34, 506–514.
Ross, D.A., Sadil, P., Wilson, D.M., Cowell, R.A., 2018. Hippocampal Engagement during Recall Depends on Memory Content. Cereb Cortex 28, 2685–2698.
Rothschild, G., Eban, E., Frank, L.M., 2017. A cortical-hippocampal-cortical loop of information processing during memory consolidation. Nat Neurosci 20, 251–259.
Schneider, D.M., Woolley, S.M., 2011. Extra-classical tuning predicts stimulus-dependent receptive fields in auditory neurons. J Neurosci 31, 11867–11878.
Schreiner, C., Winer, J.A., 2005. The inferior colliculus. Springer.
Simmons, A.M., 2003. Perspectives and progress in animal acoustic communication. In: Acoustic communication. Springer, pp. 1–14.
Sitko, A.A., Goodrich, L.V., 2021. Making sense of neural development by comparing wiring strategies for seeing and hearing. Science 371.
Spiers, H.J., Burgess, N., Hartley, T., Vargha-Khadem, F., O'Keefe, J., 2001. Bilateral hippocampal pathology impairs topographical and episodic memory but not visual pattern matching. Hippocampus 11, 715–725.
Staib, J.M., Valle, R.Della, Knox, D.K., 2018. Disruption of medial septum and diagonal bands of Broca cholinergic projections to the ventral hippocampus disrupt auditory fear memory. Neurobiol Learn Mem 152, 71–79.
Strange, B.A., Witter, M.P., Lein, E.S., Moser, E.I., 2014. Functional organization of the hippocampal longitudinal axis. Nat Rev Neurosci 15, 655–669.
Sturm, J., Nguyen, T., Kandler, K., 2014. Development of intrinsic connectivity in the central nucleus of the mouse inferior colliculus. J Neurosci 34, 15032–15046.
Suga, N., Ma, X., 2003. Multiparametric corticofugal modulation and plasticity in the auditory system. Nat Rev Neurosci 4, 783–794.
Tanaka, K.Z., et al., 2018. The hippocampal engram maps experience but not place. Science 361, 392–397.
Telensky, P., et al., 2011. Functional inactivation of the rat hippocampus disrupts avoidance of a moving object. Proc Natl Acad Sci U S A 108, 5414–5418.
Terada, S., Sakurai, Y., Nakahara, H., Fujisawa, S., 2017. Temporal and Rate Coding for Discrete Event Sequences in the Hippocampus. Neuron 94 (1248-1262), e1244.
Theunissen, F.E., Elie, J.E., 2014. Neural processing of natural sounds. Nat Rev Neurosci 15, 355–366.
Tronson, N.C., et al., 2009. Segregated populations of hippocampal principal CA1 neurons mediating conditioning and extinction of contextual fear. J Neurosci 29, 3387–3394.
van Strien, N.M., Cappaert, N.L., Witter, M.P., 2009. The anatomy of memory: an interactive overview of the parahippocampal-hippocampal network. Nat Rev Neurosci 10, 272–282.
Vega-Flores, G., et al., 2014. The GABAergic septohippocampal pathway is directly involved in internal processes related to operant reward learning. Cereb Cortex 24, 2093–2107.
Wang, X., Leong, A.T.L., Chan, R.W., Liu, Y., Wu, E.X., 2019. Thalamic low frequency activity facilitates resting-state cortical interhemispheric MRI functional connectivity. Neuroimage 201, 115985.
Winer, J.A., Schreiner, C.E., 2005. The central auditory system: a functional analysis. In: The inferior colliculus. Springer, pp. 1–68.
Winer, J.A., 2006. Decoding the auditory corticofugal systems. Hear Res 212, 1–8.
Woolley, S.M., Portfors, C.V., 2013. Conserved mechanisms of vocalization coding in mammalian and songbird auditory midbrain. Hear Res 305, 45–56.
Woolley, S.M., Portfors, C.V., 2013. Conserved mechanisms of vocalization coding in mammalian and songbird auditory midbrain. Hear Res 305, 45–56.
Woolley, S.M., Gill, P.R., Theunissen, F.E., 2006. Stimulus-dependent auditory tuning results in synchronous population coding of vocalizations in the songbird midbrain. J Neurosci 26, 2499–2512.
Xiao, C., Liu, Y., Xu, J., Gan, X., Xiao, Z., 2018. Septal and Hippocampal Neurons Contribute to Auditory Relay and Fear Conditioning. Front Cell Neurosci 12, 102.
Xiong, X.R., et al., 2015. Auditory cortex controls sound-driven innate defense behaviour through corticofugal projections to inferior colliculus. Nat Commun 6, 7224.
Zhang, G.W., et al., 2018. A Non-canonical Reticular-Limbic Central Auditory Pathway via Medial Septum Contributes to Fear Conditioning. Neuron 97 (406-417), e404.